Progress In Electromagnetics Research M, Vol. 39, 93–106, 2014

Transient Analysis of a Rectangular Cavity Containing an Interior Scatterer Using TD-EFIE With Weighted Laguerre Polynomials as Temporal Basis Functions

Dorsaf Omri* and Taoufik Aguili

Abstract—Novel 2-D Time Domain Electric Field Integral Equations (TD-EFIE) are established in order to predict transient response of a wire enclosed within a rectangular cavity. The wire and cavity are excited by an external incident transient electromagnetic wave through a slot in the cavity wall. The formulation of the TD-EFIE is based on equivalence principle and boundary conditions taking account the effect of reflection from cavity walls. The equations are efficiently solved by Method of Moments. The transient unknown coefficients of the electric current at the wire and magnetic current at the slot are approximated using a set of orthonormal temporal basis functions derived from Laguerre Polynomials. The analysis demonstration is presented to prove that the novel TD-EFIE combined to MoM is able to solve this critical problem. No late-time instability is encountered.

1. INTRODUCTION

The study of transient response of conducting cavity due to excitation through an aperture is of considerable practical interest. In fact, the transient inducing current can damage some critical components in the system.

Developed analytical and numerical methods demonstrate the importance of an accurate prediction of the cavity's behaviors and the components enclosed in this cavity in order to overcome serious problems.

However, accurate study has been presented in [1] to determine the currents excited on a wire enclosing into a rectangular cavity and excited by EM wave trough the aperture. Moreover, this problem is formulated in frequency domain, and the desired time domain currents were obtained by numerical Inverse Fourier Transform (IFT). An exact solution using this method cannot be found because convergence problems are often encountered. In [2], the singularity expansion method (SEM) is used to determine the transient response of cavity. The SEM represents a solution of problem in terms of singularities (poles) in the complex frequency plane. For early-time responses of the system, the results are acceptable but less reliable.

A thorough study of time domain electromagnetic (TD-EM) theory of metal cavity resonator is presented in [3]. The author proves the importance of TD-EM theory compared to TD harmonic theory. Therefore, the formulation of this problem by TD-EM theory is more effective. In fact, several approaches have been applied to this important and challenging task such as Finite difference Time Domain (FDTD) method and Time Domain Integral Equation (TDIE) method. Many researches [4, 5] have proven the effectiveness of TDIE compared to FDTD for transient analysis. So, the TDIE uses fewer unknowns based on surface discretization and eliminates the artificial absorbing conditions (ABC). The marching-on in time (MOT) method is usually employed to determine the solution of TDIE [6]. However, this technique suffers from late time instability. Many measures [7–10] have attempted to

Received 21 July 2014, Accepted 1 September 2014, Scheduled 17 October 2014

* Corresponding author: Dorsaf Omri (omridorsaf@yahoo.fr).

The authors are with the SysCom Laboratory, National Engineering School of Tunis, BP.37 Le Belvedere 1002, Tunis, Tunisia.

overcome this instability as the choice of appropriate temporal basis functions. In [10, 11], the authors applied the weighted Laguerre Polynomials as temporal basis functions and obtained an accurate and stable solution.

In this paper, the task is undertaken to numerically formulate and solve the problem of an aperture which excites thin wire enclosing within rectangular cavity. The aperture is exited by an external transient EM wave.

The TD-EFIE formulation of this problem is established by the combination of equivalence principle and boundary conditions. It takes into account the effects of reflection from cavity walls.

The TD-EFIE is solved using the method of moments when we introduce a spatial and temporal testing procedure. We use the piecewise triangular function associated with Dirac function as spatial basis and testing functions. To obtain a late time stable solutions, Laguerre functions are used as temporal basis and testing functions.

The paper is organized as follows. Section 2 describes the TD-EFIE formulation and the method of solving these equations. In Section 3, the analysis demonstration with various parameters is presented. Section 4 concludes this paper.

2. TD-EFIE FORMULATION

In order to predict a transient response of the wire enclosing within rectangular cavity, let us consider the basic structure of Fig. 1(a). The structure is excited by transient EM wave exterior to the cavity and is coupled to the cavity interior through slot.

In the investigation of electromagnetic problems, simplifications or approximations must be invoked to simplify the problem. Indeed, the following hypotheses are assumed: 1) The cavity walls and the wire are perfectly conducting and very thin; 2) the wire is oriented parallel to the slot; and 3) The wire ends may not be in electrical contact with the cavity walls.

The analysis is based on the equivalence principle [18] which divides the complex problem into two simpler problems as depicted in Fig. 1.

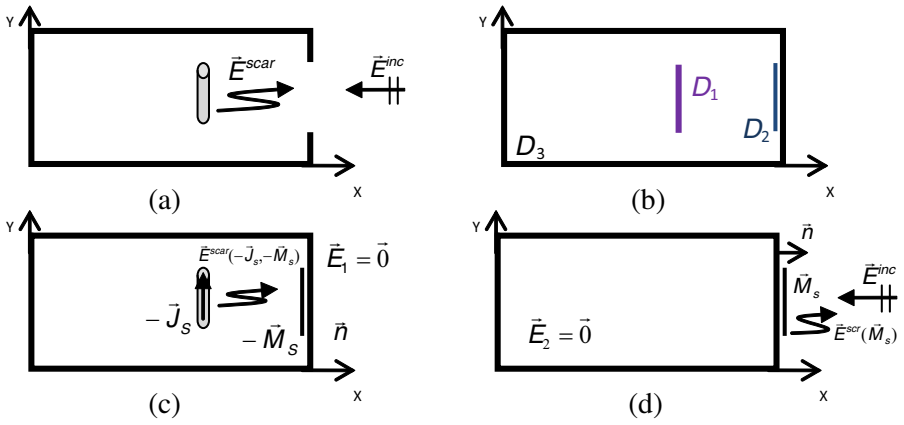

Figure 1. Analyze Problem: (a) Initial Problem; (b) Equivalent domains; (c) Internal equivalent problem; (d) External equivalent problem.

As demonstrated in [19, 20], the cavity walls and aperture are replaced by equivalent continuous domain D_3. The aperture has metalized, domain D_2. An equivalent magnetic current M_s has been introduced on it. D_2 moves an infinitesimal distance away from equivalent domain D_3. Mathematical analysis of this step shows that the aperture appears to have been short-circuited. Finally, the wire scattered is replaced by an equivalent domain D_1, and an equivalent electric current density J_s has been introduced on it.

As shown in Fig. 1(d), the total field is determined by the incident field and the equivalent magnetic current M_s over the slot. In the internal region, Fig. 1(c), the field is founded by equivalent electric — J_s over the wire and equivalent magnetic current — M_s. In both regions, the fields must satisfy the

boundary condition:

$$p\vec{M}_s = -\vec{n} \times \vec{E}^{total} \tag{1}$$

The external equivalent problem: $\begin{cases} \vec{E}^{total} = \vec{E}^1 = \vec{E}^{scar}(\vec{M}_s) + \vec{E}^{inc} \\ \vec{E}^2 = \vec{0} \\ p = +1 \end{cases}$. The internal equivalent problem: $\begin{cases} \vec{E}^{total} = \vec{E}^2 = \vec{E}^{scar}(-\vec{M}_s) + \vec{E}^{scar}(-\vec{J}_s) \\ \vec{E}^1 = \vec{0} \\ p = -1 \end{cases}$.

Now, we force the boundary condition. So, the tangential electric field must vanish in the surface of the wire and in the cavity walls:

$$\left[\vec{E}^{scar}(-\vec{J}_s) + \vec{E}^{scar}(-\vec{M}_s)\right]_{\tan} = 0 \ over \ D_1 \tag{2}$$

$$\left[\vec{E}^{scar}(-\vec{J}_s) + \vec{E}^{scar}(-\vec{M}_s)\right]_{\tan} = 0 \ over \ D_3 \tag{3}$$

The tangential component of the electric field is continuous across equivalent domain D_2 ($\vec{n} \times \vec{E}^1 = \vec{n} \times \vec{E}^2$). Therefore, we obtain the following equation:

$$\left[\vec{E}^{inc} + \vec{E}^{scar}(\vec{M}_s)\right]_{\tan} = \left[\vec{E}^{scar}(-\vec{J}_s) + \vec{E}^{scar}(-\vec{M}_s)\right]_{\tan} over \ D_2 \tag{4}$$

where

$$\vec{E}^{scar}(\vec{M}_s) = -\frac{1}{\varepsilon}\nabla \times \vec{F} \tag{5}$$

$$\vec{E}^{scar}(\vec{J}_s) = -\frac{\partial}{\partial t}\vec{A} - \nabla\varphi \tag{6}$$

A, φ and F are the electric vector potential, electric scalar potential and magnetic vector potential, respectively and given by:

$$\vec{A}(x,y,t) = \frac{\mu}{4\pi}\iint\limits_{D_j} \frac{\vec{J}_s(x',y',t-{}^{R_{ij}}/_{C})}{R_{ij}}ds' \tag{7}$$

$$\varphi(x,y,t) = \frac{1}{4\pi\varepsilon}\iint\limits_{D_j} \frac{q_s(x',y',t-{}^{R_{ij}}/_{C})}{R_{ij}}ds' \tag{8}$$

$$\vec{F}(x,y,t) = \frac{\varepsilon}{4\pi}\iint\limits_{D_j} \frac{\vec{M}_s(x',y',t-{}^{R_{ij}}/_{C})}{R_{ij}}ds' \tag{9}$$

In (7), (8) and (9), μ, ε and C are the permeability, permittivity and velocity of propagation of electromagnetic wave, in free space. (x, y) and (x', y') are the observation and source points. $t - \frac{R_{ij}}{C}$ represents the retarded time. R_{ij} is the distance between the observation point (defined on the domain D_i) and the source point (defined on the domain D_j):

$$R_{ij} = \sqrt{(x-x')^2 + (y-y')^2}$$

Based on Equations (2)–(6) and the expressions of scalar and vector potentials described above, we can establish the following equations:

$$\left[-\frac{\mu}{4\pi}\frac{\partial}{\partial t}\iint\limits_{D_1}\frac{\vec{J}_s(x',y',t-{}^{R_{11}}/_{C})}{R_{11}(x,y,x',y')}ds' - \frac{1}{4\pi\varepsilon}\iint\limits_{D_1}\frac{\nabla\cdot\varphi(x',y',t-{}^{R_{11}}/_{C})}{R_{11}(x,y,x',y')}\right.$$

$$\left.-\frac{1}{4\pi}\nabla\times\iint\limits_{D_2}\frac{\vec{M}_s(x',y',t-{}^{R_{12}}/_{C})}{R_{12}(x,y,x',y')}ds'\right] = \vec{0} \tag{10}$$

$$\left[-\frac{\mu}{4\pi}\frac{\partial}{\partial t}\iint\limits_{D_1}\frac{\vec{J}_s(x',y',t-{}^{R_{21}}\!/_C)}{R_{21}(x,y,x',y')}ds'-\frac{1}{4\pi\varepsilon}\iint\limits_{D_1}\frac{\nabla\cdot\varphi(x',y',t-{}^{R_{21}}\!/_C)}{R_{21}(x,y,x',y')}\right.$$
$$\left.-\frac{2}{4\pi}\nabla\times\iint\limits_{D_2}\frac{\vec{\vec{M}}_s(x',y',t-{}^{R_{22}}\!/_C)}{R_{22}(x,y,x',y')}ds'\right]=E^{inc}(x,y,t) \tag{11}$$

$$\left[-\frac{\mu}{4\pi}\frac{\partial}{\partial t}\iint\limits_{D_1}\frac{\vec{J}_s(x',y',t-{}^{R_{31}}\!/_C)}{R_{31}(x,y,x',y')}ds'-\frac{1}{4\pi\varepsilon}\iint\limits_{D_1}\frac{\nabla\cdot\varphi(x',y',t-{}^{R_{31}}\!/_C)}{R_{31}(x,y,x',y')}\right.$$
$$\left.-\frac{1}{4\pi}\nabla\times\iint\limits_{D_2}\frac{\vec{\vec{M}}_s(x',y',t-{}^{R_{32}}\!/_C)}{R_{32}(x,y,x',y')}ds'\right]=\vec{0} \tag{12}$$

The TD-EFIE are solved in space and time domains by applying the method of moments [16].

2.1. Spatial Expansion and Testing

Domain D_1, which will be analyzed, is approximated by Piecewise Rectangular Function [17] associated with Dirac function. The spatial basis function at the nth point is defined by $\vec{f}_n=\Re_n\cdot\Lambda_{\chi_j}\vec{u}$ where

$$\Re_k(h)=\begin{cases}\dfrac{h-h_{k-1}}{h_k-h_{k-1}}, & h\in[h_{k-1},h_k]\\ \dfrac{h_{k+1}-h}{h_{k+1}-h_k}, & h\in[h_k,h_{k+1}]\\ 0, & \text{otherwise}\end{cases}\qquad \Lambda_{\chi_j}(\chi)=\begin{cases}1, & \chi=\chi_j\\ 0, & \text{otherwise}\end{cases} \tag{13}$$

Domain D_2 is approximated by another vector basis function and is defined by: $\vec{g}_n(x,y)=\vec{n}\times\vec{f}_n(x,y)=\vec{n}\times(\Re_n(y)\cdot\Lambda_{x_S}(x)\vec{y})$ where $\vec{n}$ is the unit normal pointing outward from the equivalent surface D_3. The unknown electric and magnetic currents $\vec{J}_s(x,y,t)$ and $\vec{M}_s(x,y,t)$ on the wire and slot, respectively, may be approximated in terms of two separate spatial basis functions as:

$$\vec{J}_s(x,y,t)=\sum_{n=1}^{N_w}J_n(t)\vec{f}_n(x,y)\ where\ \vec{f}_n(x,y)=\Re_n(y)\cdot\Lambda_{x_w}(x)\vec{y} \tag{14}$$

$$\vec{M}_s(x,y,t)=\sum_{n=1}^{N_s}M_n(t)\vec{g}_n(x,y) \tag{15}$$

In the present work, the slot and wire are subdivided into N_s and N_w sub-domains using the expansion functions (13) in y-direction. The length of each segment Δy is fixed. In x-direction, the wire and slot are fixed at points X_s and X_w. The cavity walls are divided into $N_c=N_{c-x}\times N_{c-y}$ sub-domains using testing function $\vec{h}_n$ which is defined by:

$$h_k(x,y)=\begin{cases}f_k(x_1,y),\ y\in[y_k,y_{k+1}],\ k\in\{1\ \ldots\ N_{c-y}\}\\ f_k(x_{N_{c-x}},y),\ y\in[y_k,y_{k+1}],\ k\in\{1\ \ldots\ N_{c-y}\}\\ f_k(x,y),\ y\in[y_1,y_2],\ x=x_k,\ k\in\{1\ \ldots\ N_{c-x}\}\\ f_k(x,y),\ y\in\left[y_{N_{c-y}}-1,y_{N_{c-y}}\right],\ x=x_k,\ k\in\{1\ \ldots\ N_{c-x}\}\end{cases} \tag{16}$$

In order to avoid a time integral term in (10), (11) and (12) and to handle the time derivative of the electric potential vector, we introduce the Hertz vector [11]:

$$\vec{J}_s(x,y,t)=\frac{d}{dt}\zeta_s(x,y,t) \tag{17}$$

The relation between the vector hertz and the electric scalar potential is given by:

$$\varphi(x,y,t) = -\nabla \cdot \vec{\zeta}_s(x,y,t) \tag{18}$$

We define another Hertz vector for the magnetic current as:

$$\vec{M}_s(x,y,t) = \frac{d}{dt}\vec{\vartheta}_s(x,y,t) \tag{19}$$

Based on (14) and (15), we may expand the two unknown sources $\vec{\zeta}_s$ and $\vec{\vartheta}_s$ as:

$$\vec{\zeta}_s(x,y,t) = \sum_{n=1}^{N_w} \zeta_n(t)\vec{f}_n(x,y) \tag{20}$$

$$\vec{\vartheta}_s(x,y,t) = \sum_{n=1}^{N_s} \vartheta_n(t)\vec{g}_n(x,y) \tag{21}$$

Using MoM, we develop a testing procedure associated to expansion procedure, already developed above with (13), (20) and (21). By choosing the adequate testing functions and using the appropriate scalar product, we obtain:

$$\left[\sum_{n=1}^{N_w}\left[-\mu a_{mn}^{11}\frac{d^2\zeta_n(t-R_{mn}^{11}/C)}{dt^2} + \frac{b_{mn}^{11}}{\varepsilon}\zeta_n(t-R_{mn}^{11}/C)\right] + \sum_{n=1}^{N_S} -c_{mn}^{21}\frac{d\upsilon_n(t-R_{mn}^{21}/C)}{dt}\right] = 0 \tag{22}$$

$$\left[\sum_{n=1}^{N_w}\left[-\mu a_{mn}^{12}\frac{d^2\zeta_n(t-R_{mn}^{12}/C)}{dt^2} + \frac{b_{mn}^{12}}{\varepsilon}\zeta_n(t-R_{mn}^{12}/C)\right] + 2\sum_{n=1}^{N_S} -c_{mn}^{22}\frac{d\upsilon_n(t-R_{mn}^{22}/C)}{dt}\right] = E_m^{inc}(t) \tag{23}$$

$$\left[\sum_{n=1}^{N_w}\left[-\mu a_{mn}^{13}\frac{d^2\zeta_n(t-R_{mn}^{13}/C)}{dt^2} + \frac{b_{mn}^{13}}{\varepsilon}\zeta_n(t-R_{mn}^{13}/C)\right] + \sum_{n=1}^{N_S} -c_{mn}^{23}\frac{d\upsilon_n(t-R_{mn}^{23}/C)}{dt}\right] = 0 \tag{24}$$

a_{mn}^{ij}, b_{mn}^{ij}, c_{mn}^{ij} and $E_m^{inc}(t)$ are developed in Appendix A.

We assume that the unknown transient quantities ζ_n and υ_n do not change appreciably within the segment Δy, whose length is very small, so that $\tau^{ij} = t - R^{ij}(x,y,x',y')/C \rightarrow \tau_{mn}^{ij} = t - R_{mn}^{ij}/C$.

2.2. Temporal Expansion and Testing

The time coefficients $\zeta_n(t)$ and $\upsilon_n(t)$ in (20) and (21) can be expanded using weighted Laguerre Polynomial as temporal basis function. We define these coefficients as:

$$\zeta_n(t) = \sum_{a=0}^{\infty} \zeta_{n,a}\varphi_a(st) \tag{25}$$

$$\upsilon_n(t) = \sum_{a=0}^{\infty} \upsilon_{n,a}\varphi_a(st) \tag{26}$$

where

$$\varphi_a(st) = e^{-st/2}L_a(st) \tag{27}$$

$L_a(st)$ is the Laguerre Polynomial of order "a". "s" is a scaling factor [14]. The various mathematical properties of these functions are introduced in [10–15]. We assume that the time responses $\left\{\zeta_n(t), \frac{d\zeta_n(t)}{dt}\right\}$ and $\left\{\upsilon_n(t), \frac{d\upsilon_n(t)}{dt}\right\}$ at $t = 0$ have not started yet due to the casualty.

After the conventional temporal testing procedure with Galerkin's method for the bth order of Laguerre function and using the expression of expanding the first and second derivative of transient

coefficients presented in [11], we obtain the following time domain equations derived from (22), (23) and (24):

$$\left[\begin{array}{l}\displaystyle\sum_{n=1}^{N_w}\left[\begin{array}{l}-s^2\mu a_{mn}^{11}\displaystyle\sum_{a=0}^{b}\left[\frac{1}{4}\zeta_{n,a}+\sum_{k=0}^{a-1}(a-k)\zeta_{n,k}\right]I_{ba}\left(s\left({}^{R_{mn}^{11}}\!/_{C}\right)\right)\\ +\dfrac{b_{mn}^{11}}{\varepsilon}\displaystyle\sum_{a=0}^{b}\zeta_{n,a}I_{ba}\left(s\left({}^{R_{mn}^{11}}\!/_{C}\right)\right)\end{array}\right]\\ +\displaystyle\sum_{n=1}^{N_S}-sc_{mn}^{21}\sum_{a=0}^{b}\left[\frac{1}{2}\upsilon_{n,a}+\sum_{k=0}^{a-1}\upsilon_{n,k}\right]I_{ba}\left(s\left({}^{R_{mn}^{21}}\!/_{C}\right)\right)\end{array}\right]=0 \tag{28}$$

$$\left[\begin{array}{l}\displaystyle\sum_{n=1}^{N_w}\left[\begin{array}{l}-s^2\mu a_{mn}^{12}\displaystyle\sum_{a=0}^{b}\left[\frac{1}{4}\zeta_{n,a}+\sum_{k=0}^{a-1}(a-k)\zeta_{n,k}\right]I_{ba}\left(s\left({}^{R_{mn}^{12}}\!/_{C}\right)\right)\\ +\dfrac{b_{mn}^{12}}{\varepsilon}\displaystyle\sum_{a=0}^{b}\zeta_{n,a}I_{ba}\left(s\left({}^{R_{mn}^{12}}\!/_{C}\right)\right)\end{array}\right]\\ +2\displaystyle\sum_{n=1}^{N_S}-sc_{mn}^{22}\sum_{a=0}^{b}\left[\frac{1}{2}\upsilon_{n,a}+\sum_{k=0}^{a-1}\upsilon_{n,k}\right]I_{ba}\left(s\left({}^{R_{mn}^{22}}\!/_{C}\right)\right)\end{array}\right]=E_{m,b}^{inc} \tag{29}$$

$$\left[\begin{array}{l}\displaystyle\sum_{n=1}^{N_w}\left[\begin{array}{l}-s^2\mu a_{mn}^{13}\displaystyle\sum_{a=0}^{b}\left[\frac{1}{4}\zeta_{n,a}+\sum_{k=0}^{a-1}(a-k)\zeta_{n,k}\right]I_{ba}\left(s\left({}^{R_{mn}^{13}}\!/_{C}\right)\right)\\ +\dfrac{b_{mn}^{13}}{\varepsilon}\displaystyle\sum_{a=0}^{b}\zeta_{n,a}I_{ba}\left(s\left({}^{R_{mn}^{13}}\!/_{C}\right)\right)\end{array}\right]\\ +\displaystyle\sum_{n=1}^{N_S}-sc_{mn}^{23}\sum_{a=0}^{b}\left[\frac{1}{2}\upsilon_{n,a}+\sum_{k=0}^{a-1}\upsilon_{n,k}\right]I_{ba}\left(s\left({}^{R_{mn}^{23}}\!/_{C}\right)\right)\end{array}\right]=0 \tag{30}$$

where

$$\begin{aligned}I_{ba}\left(s\frac{R_{mn}^{ij}}{C}\right)&=\left\langle\varphi_b(st),\varphi_a\left(s\left(t-\frac{R_{mn}^{ij}}{C}\right)\right)\right\rangle=\int_0^{\infty}\varphi_b(st)\varphi_a\left(s\left(t-\frac{R_{mn}^{ij}}{C}\right)\right)d(st)\\&=\left\{\begin{array}{l}e^{-\frac{sR_{mn}}{2C}}\left[L_{b-a}(s\frac{R_{mn}}{C})-L_{b-a-1}(s\frac{R_{mn}}{C})\right],\ a\le b\\0,\ a>b\end{array}\right.\end{aligned} \tag{31}$$

and

$$E_{b,m}^{inc}=\int_0^{\infty}\varphi_b(st)E_m^{inc}(t)d(st) \tag{32}$$

Based on the orthogonality condition of Laguerre functions, we can change the upper limit of the sum (25) and (26) from ∞ to "b" as expressed in (28), (29) and (30). In the same equations, we move the terms including the transient unknown coefficients which are known for $a<b$, to right-hand side. So, we rewrite the resulting equations in a simple form:

$$\left\{\begin{array}{ll}\displaystyle\sum_{n=1}^{N_w}A_{mn}^{11}\zeta_{n,b}+\sum_{n=1}^{N_s}B_{mn}^{21}\upsilon_{n,b}=T_{m,b}^{1} & \text{(a)}\\ \displaystyle\sum_{n=1}^{N_w}A_{mn}^{12}\zeta_{n,b}+\sum_{n=1}^{N_s}B_{mn}^{22}\upsilon_{n,b}=E_{m,b}^{inc}+T_{m,b}^{2} & \text{(b)}\\ \displaystyle\sum_{n=1}^{N_w}A_{mn}^{13}\zeta_{n,b}+\sum_{n=1}^{N_s}B_{mn}^{23}\upsilon_{n,b}=T_{m,b}^{3} & \text{(c)}\end{array}\right. \tag{33}$$

The space matrix A^{ij}, B^{ij} and the retarded terms T_b^j are presented in Appendices A and B, respectively.

Finally, we can write (33) in a matrix form as:

$$\begin{bmatrix} A^{11} & B^{21} \\ A^{12} & B^{22} \\ A^{13} & B^{23} \end{bmatrix} \begin{bmatrix} \zeta_b \\ \upsilon_b \end{bmatrix} = \begin{bmatrix} T_b^1 \\ -E_b^{inc} + T_b^2 \\ T_b^3 \end{bmatrix} \tag{34}$$

Equation (34) is not a function of temporal testing function. Therefore, we can solve the matrix equation as increasing the degree of temporal testing functions which leads to solving the problem only in space for each degree of Laguerre function. Once the unknown coefficients ζ_n and υ_n are solved, the transient electric and magnetic current densities can be obtained by:

$$\begin{cases} J_n(t) = \dfrac{d}{dt}\zeta_n(t) = s\displaystyle\sum_{a=0}^{A}\left[\frac{1}{2}\zeta_{n,a} + \sum_{k=0}^{a-1}\zeta_{n,k}\right]\varphi_a(st) \\ \vec{J}_s(x,y,t) = \displaystyle\sum_{n=1}^{N_w} J_n(t)\vec{f}_n(x,y) \end{cases} \tag{35}$$

$$\begin{cases} M_n(t) = \dfrac{d}{dt}\upsilon_n(t) = s\displaystyle\sum_{a=0}^{A}\left[\frac{1}{2}\upsilon_{n,a} + \sum_{k=0}^{a-1}\upsilon_{n,k}\right]\varphi_a(st) \\ \vec{M}_s(x,y,t) = \displaystyle\sum_{n=1}^{N_S} M_n(t)\vec{g}_n(x,y) \end{cases} \tag{36}$$

A is the maximum order of Laguerre functions [12].

3. NUMERICAL RESULTS

In this section, we give a quantitative discussion concerning the transient response of the cavity containing an interior scatterer. In the following, we present different numerical results for various parameters: slot length, slot offset, separate distance and wire length.

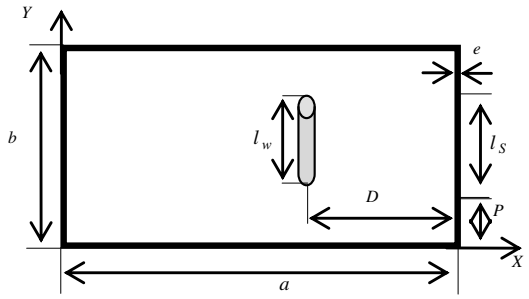

Figure 2. The geometrical parameters of the problem are: $a = 2 * b\,\text{mm}$, $b = 109.3\,\text{mm}$, $D = 43.7\,\text{mm}$, $P = 32.8\,\text{mm}$, $l_w = l_s = 39.5\,\text{mm}$ and $e = e_w = 10^{-5}\,\text{mm}$ (e_w is the thickness of wire).

Figure 2 shows the structure of the problem. The cavity is excited through the slot by rectangular pulse [10] which is defined by:

$$E^{inc}(x,y,t) = \begin{cases} 1, & 10^{-9}s \le t \le 10^{-8}s \\ 0, & \text{others} \end{cases} \tag{37}$$

We subdivide the cavity walls into $N_{c-x} \times N_{c-y} = 200 \times 200$ segments of length $\Delta_x \times \Delta_y = \frac{a}{N_{c-x}} \times \frac{b}{N_{c-y}}$. Thus, the wire and slot are divided into $N_w \approx \frac{l_w}{\Delta_y}$ and $N_s \approx \frac{l_s}{\Delta_y}$ sub-domains, respectively.

3.1. Shielding of the Cavity

In order to carry through our propose formulation, we start by studying the transient electromagnetic scattering from thin wire excited by EM wave (37) in free space. Fig. 3(a) shows the transient current induced at the center of the wire scatterer as function of time, and Fig. 3(b) shows the spatial distribution of the current at $t = 1.3^{*}10^{-9}s$ which applies same formulation, described in [10].

Figures 3(c) and (d) depict the transient response of the same wire enclosing in the cavity as shown in Fig. 2. The wire is excited by the same source through the aperture. The two transient responses are different due to the cavity's shielding. The space distribution of the current at the wire is close to that presented in [1].

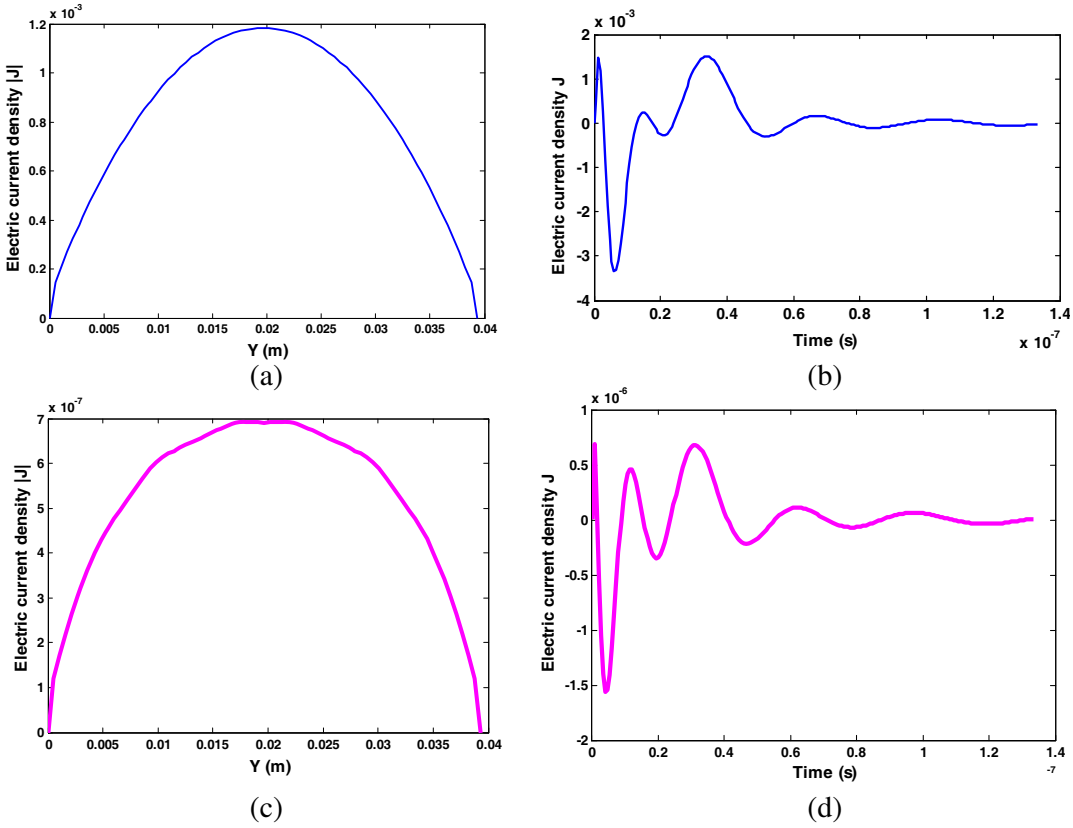

Figure 3. Transient response of the wire: (a) Space distribution of electric current density in free space; (b) Electric current density at the center of the wire in free space at $t = 1.3 * 10^{-9}$ s; (c) Space distribution of electric current density of the wire enclosing within rectangular cavity; (d) Electric current density at the center of the wire enclosing within rectangular cavity at $t = 1.3 * 10^{-9}$ s.

We also note that the amplitude of the current density in free space has a peak at approximately 3.3 mA that decreases to the order of 1.5 µA inside the cavity. Thus the shielding of the cavity significantly reduces the currents.

3.2. Slot Length

The transient responses of the wire and slot for various sizes of slot are revealed. The separate distance D, the cavity size, the wire length l_w and the distance P are fixed, as shown in Fig. 4. So there are three varied slot lengths.

The transient electric current at the center of the wire and the transient magnetic current at the center of the slot become more important when the length of the slot is increased, as depicted in Fig. 5 and Fig. 6(a).

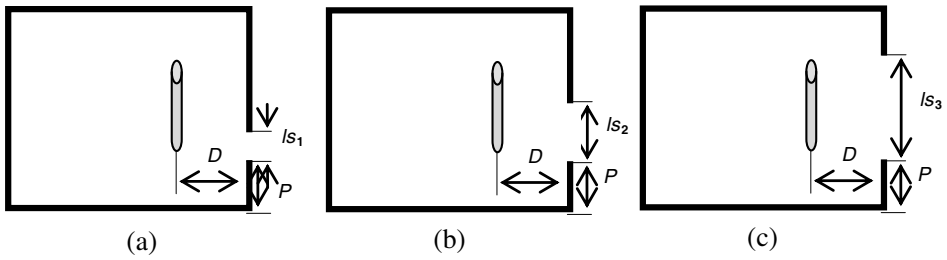

Figure 4. Various slot lengths: (a) $ls_1 = 0.25 * ls$; (b) $ls_2 = 0.5 * ls$; (c) $ls_3 = ls$.

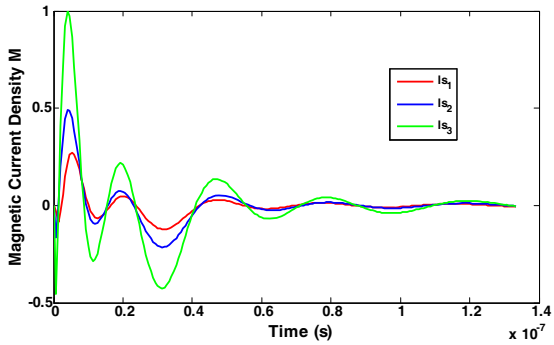

Figure 5. The normalized magnetic current density at the center of the slot for various slot lengths.

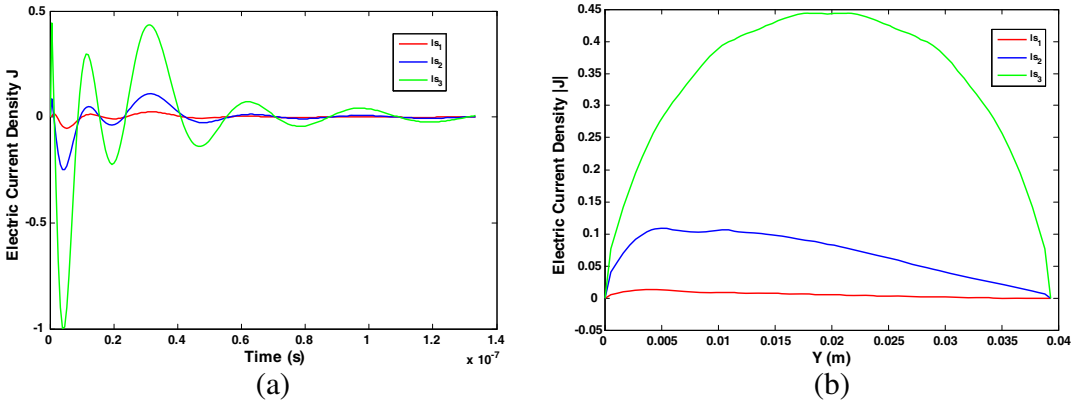

Figure 6. Transient response of the wire for various slot lengths: (a) The normalized electric current density at the center of the wire; (b) The normalized space current distribution of the wire at $t = 1.3 * 10^{-9}$ s.

As physically expected, the length of the slot has an impact on space distribution of current on the wire, as presented in Fig. 6(b). Hence, the blue curve shows that the magnitude of the electric current vanishes in the absence of the slot.

3.3. Slot Offset

The position of slot P, referred to as the slot offset, is of variable interest. Thus, when we change position P, the magnitude of current varies significantly. Transient electric current density at the center of the wire for various slot positions: P_1, P_2 and P_3 is shown in Fig. 7(a) (the wire and slot have the same length). The position of the wire and separate distance D are fixed. In fact, the magnitude of current density is increased when the slot is located at the center of the cavity wall, position P_2. But, when the slot is located at the bottom or the top of cavity wall, positions P_1 and P_3, respectively, the currents densities have the same variation.

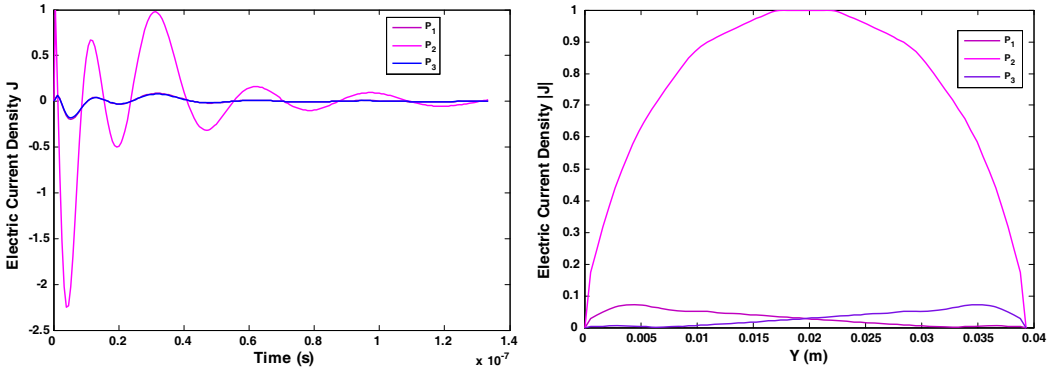

Figure 7. Transient response of the wire for various slot positions: ($P_1 = 10.9\,\text{mm}$, the corresponding slot offset = (218.5 mm, 30.7 mm)), ($P_2 = 328\,\text{mm}$, the corresponding slot offset = (218.5 mm, 525 mm)) and ($P_3 = 54.6\,\text{mm}$, the corresponding slot offset = (218.5 mm, 744 mm)): (a) The normalized transient current at the center of the wire; (b) The normalized space distribution of the current density at $t = 1.3 * 10^{-9}\,\text{s}$.

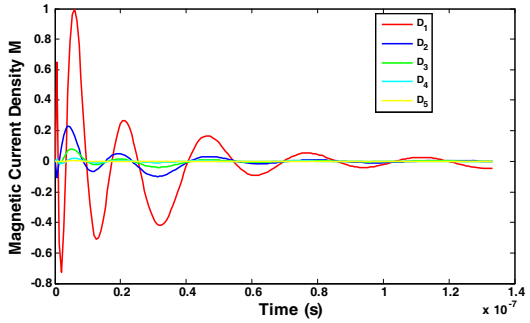

Figure 8. The normalized magnetic current at the center of the slot for various separate distances D.

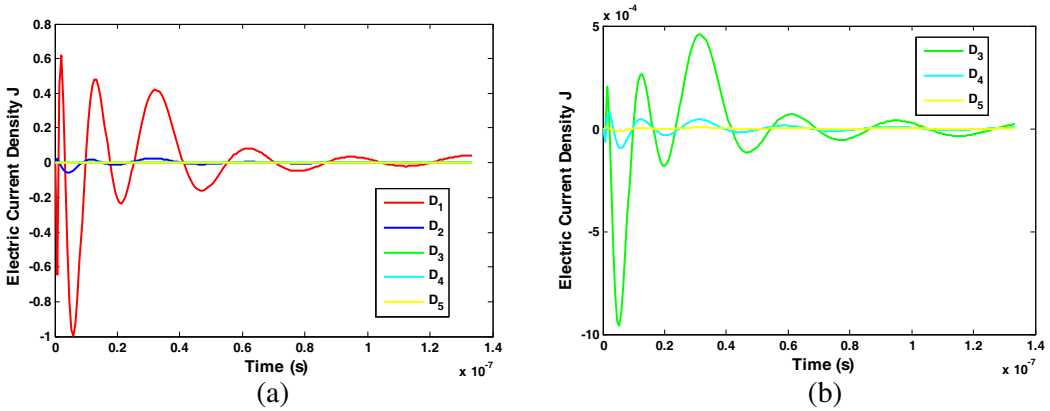

Figure 9. Transient response of the wire for various separate distances D: (a) The normalized electric current density at the center of the wire; (b) The normalized electric current density at the center of the wire for higher distances.

Indeed, the space distributions of the current on the wire, for the three positions, are different, as shown in Fig. 7(b). We notice that when the slot is located on the bottom of the cavity wall, the magnitude of current density is maximal at the bottom of the wire and vanishes at the top. So, when the slot is located at the top of the cavity wall, the magnitude of current density is maximal at the top of wire and vanishes at the bottom.

3.4. Wire Location

In order to study the coupling between wireslot and to demonstrate the influence of the separate distance D to the behaviours of electric and magnetic currents, we consider five distances D: $D_1 = 0.01 \times a$, $D_2 = 0.1 \times a$, $D_3 = 0.5 \times a$, $D_4 = 0.7 \times a$ and $D_5 = 0.9 \times a$.

Figures 8 and 9 show the transient responses of the slot and wire for different locations of the wire. It is physically evident that when the wire is moved further from the slot, the magnitude of electric and magnetic current densities become lower. Fig. 9(b) demonstrates that even if the wire is estranged from the slot, there is lower variation of electric current density at the center of the wire. This variation can be explained mathematically by the coupling matrix A^{12} and B^{21} in (33). $||A^{12}||$ and $||B^{21}||$ increase when the separate distance D is lower (see Equations (A3), (A4) and (A5) in Appendix A).

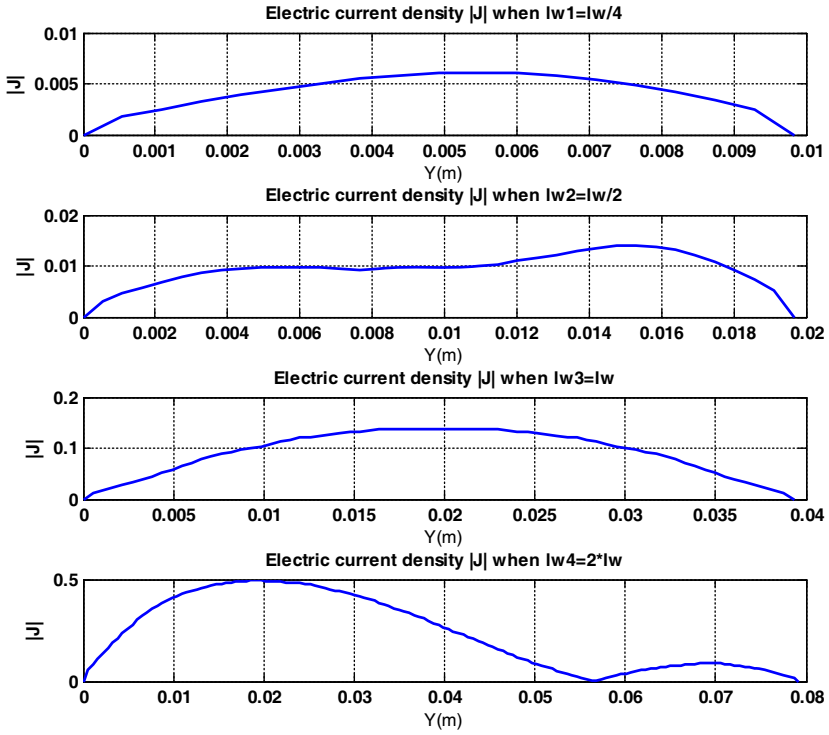

Figure 10. Space distribution of electric current density at $t = 1.3 * 10^{-9}$ s for various wire lengths.

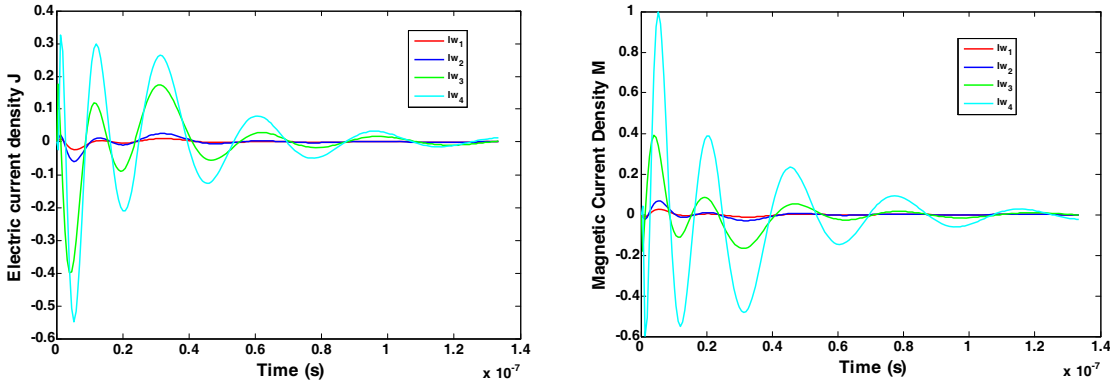

Figure 11. Transient response of the wire and slot wire for various wire lengths: (a) Normalized electric current at the center of the wire; (b) Normalized magnetic current at the center of the slot.

3.5. Wire Length

In order to demonstrate the influence of the wire length on the behaviour of the transient electric and magnetic current, we consider four lengths: $lw_1 = lw/4$, $lw_2 = lw/2$, $lw_3 = lw$ and $lw_4 = 2 * lw$. The length of the slot, separate distance D, position of the wire, position of the slot and cavity size are fixed as presented in Fig. 2 (we note that the wire and slot have the same position P).

As depicted in Fig. 10, the space distribution on the wire varies when the length of wire changes.

The relation between the wire length and the transient response of the wire and slot is revealed in Fig. 11. The magnitude of electric and magnetic current densities becomes higher as the length of the wire grows.

4. CONCLUSION

In this paper, we have applied the equivalence principle combined to boundary conditions to develop a novel 2-D numerical time domain integral equations for studding the transient behavior of thin wire enclosing within rectangular cavity and excited by transient EM wave through the slot.

TD-EFIE is successfully solved by application of the MoM in space and time domain. Accurate spatial basis and testing functions are used. We introduce a temporal basis and testing functions set derived from Laguerre polynomials.

Stable and accurate results have mainly been found with electric and magnetic currents responses.

This formulation can be extended to 3-D and is easily applicable to study various cavity related problems.

APPENDIX A.

The space matrix A_{mn}^{ij} and B_{mn}^{ij} can be defined by:

$$A_{mn}^{ij} = \left(-s^2 \frac{\mu a_{mn}^{ij}}{4} + \frac{b_{mn}^{ij}}{\varepsilon}\right) I_{bb}\left(s\left(R_{mn}^{ij}/C\right)\right) \tag{A1}$$

$$B_{mn}^{ij} = -\frac{s c_{mn}^{ij}}{2} I_{bb}\left(s\left(R_{mn}^{ij}/C\right)\right) \tag{A2}$$

where

$$In\ (22): \begin{cases} a_{mn}^{11} = \left\langle f_m(x,y), \dfrac{1}{4\pi} \iint\limits_{D_1} \dfrac{f_n(x',y')}{R_{11}(x,y,x',y')} ds' \right\rangle \\ b_{mn}^{11} = \left\langle f_m(x,y), \dfrac{1}{4\pi} \nabla \iint\limits_{D_1} \dfrac{\nabla f_n(x',y')}{R_{11}(x,y,x',y')} ds' \right\rangle \\ c_{mn}^{21} = \left\langle f_m(x,y), \dfrac{1}{4\pi} \nabla \times \iint\limits_{D_2} \dfrac{g_m(x',y')}{R_{21}(x,y,x',y')} ds' \right\rangle \end{cases} \tag{A3}$$

$$In\,(23): \begin{cases} a_{mn}^{12} = \left\langle g_m(x,y), \dfrac{1}{4\pi} \iint\limits_{D_1} \dfrac{f_n(x',y')}{R_{12}(x,y,x',y')} ds' \right\rangle \\ b_{mn}^{12} = \left\langle g_m(x,y), \dfrac{1}{4\pi} \nabla \iint\limits_{D_1} \dfrac{\nabla f_n(x',y')}{R_{12}(x,y,x',y')} ds' \right\rangle \\ c_{mn}^{22} = \left\langle g_m(x,y), \dfrac{1}{4\pi} \nabla \times \iint\limits_{D_2} \dfrac{g_m(x',y')}{R_{22}(x,y,x',y')} ds' \right\rangle \end{cases} \tag{A4}$$

$$In\ (24):\ \begin{cases} a_{mn}^{13} = \left\langle h_m(x,y), \dfrac{1}{4\pi}\displaystyle\iint_{D_1} \dfrac{f_n(x',y')}{R_{13}(x,y,x',y')}ds' \right\rangle \\ b_{mn}^{13} = \left\langle h_m(x,y), \dfrac{1}{4\pi}\nabla\displaystyle\iint_{D_1} \dfrac{\nabla f_n(x',y')}{R_{13}(x,y,x',y')}ds' \right\rangle \\ c_{mn}^{23} = \left\langle h_m(x,y), \dfrac{1}{4\pi}\nabla\times\displaystyle\iint_{D_2} \dfrac{g_m(x',y')}{R_{23}(x,y,x',y')}ds' \right\rangle \end{cases} \tag{A5}$$

$$I_{bb}\left(s\left(R_{mn}^{ij}/C\right)\right) = e^{-\frac{s}{2}\left(R_{mn}^{ij}/C\right)} \tag{A6}$$

The projection of the source is given by:

$$\vec{E}^{inc}(t) = \left\langle \vec{g}_(x,y), \vec{n}\times\vec{E}^{inc}(x,y,t)\right\rangle = \iint_{D_2} \vec{g}_(x,y)\cdot\left[\vec{n}\times\vec{E}^{inc}(x,y,t)\right]ds \tag{A7}$$

APPENDIX B.

The retarded terms take the following forms:

$$T_{m,b}^{1} = -\left[\begin{array}{l} \displaystyle\sum_{n=1}^{N_w}\left[-s^2\mu a_{mn}^{11}\sum_{k=0}^{b-1}(b-k)\zeta_{n,k}I_{bb}\left(s\left(R_{mn}^{11}/C\right)\right)\right] \\ \displaystyle\sum_{n=1}^{N_w}\left[-s^2\mu a_{mn}^{11}\sum_{a=0}^{b-1}\left[\frac{1}{4}\zeta_{n,a}+\sum_{k=0}^{a-1}(a-k)\zeta_{n,k}\right]I_{ab}\left(s\left(R_{mn}^{11}/C\right)\right)+\frac{b_{mn}^{11}}{\varepsilon}\sum_{a=0}^{b-1}\zeta_{n,a}I_{ab}\left(s\left(R_{mn}^{11}/C\right)\right)\right] \\ +\displaystyle\sum_{n=1}^{N_s}-sc_{mn}^{21}\sum_{k=0}^{b-1}\upsilon_{n,k}I_{bb}\left(s\left(R_{mn}^{21}/C\right)\right)+\sum_{n=1}^{N_s}-sc_{mn}^{21}\sum_{a=0}^{b-1}\left[\frac{1}{2}\upsilon_{n,a}+\sum_{k=0}^{a-1}\upsilon_{n,k}\right]I_{ab}\left(s\left(R_{mn}^{21}/C\right)\right) \end{array}\right] \tag{B1}$$

$$T_{m,b}^{2} = -\left[\begin{array}{l} \displaystyle\sum_{n=1}^{N_w}\left[-s^2\mu a_{mn}^{12}\sum_{k=0}^{b-1}(b-k)\zeta_{n,k}I_{bb}\left(s\left(R_{mn}^{12}/C\right)\right)\right] \\ \displaystyle\sum_{n=1}^{N_w}\left[-s^2\mu a_{mn}^{12}\sum_{a=0}^{b-1}\left[\frac{1}{4}\zeta_{n,a}+\sum_{k=0}^{a-1}(a-k)\zeta_{n,k}\right]I_{ab}\left(s\left(R_{mn}^{12}/C\right)\right)+\frac{b_{mn}^{12}}{\varepsilon}\sum_{a=0}^{b-1}\zeta_{n,a}I_{ab}\left(s\left(R_{mn}^{12}/C\right)\right)\right] \\ +2\displaystyle\sum_{n=1}^{N_s}-sc_{mn}^{22}\sum_{k=0}^{b-1}\upsilon_{n,k}I_{bb}\left(s\left(R_{mn}^{22}/C\right)\right)+2\sum_{n=1}^{N_s}-sc_{mn}^{22}\sum_{a=0}^{b-1}\left[\frac{1}{2}\upsilon_{n,a}+\sum_{k=0}^{a-1}\upsilon_{n,k}\right]I_{ab}\left(s\left(R_{mn}^{22}/C\right)\right) \end{array}\right] \tag{B2}$$

$$T_{m,b}^{3} = -\left[\begin{array}{l} \displaystyle\sum_{n=1}^{N_w}\left[-s^2\mu a_{mn}^{13}\sum_{k=0}^{b-1}(b-k)\zeta_{n,k}I_{bb}\left(s\left(R_{mn}^{13}/C\right)\right)\right] \\ \displaystyle\sum_{n=1}^{N_w}\left[-s^2\mu a_{mn}^{13}\sum_{a=0}^{b-1}\left[\frac{1}{4}\zeta_{n,a}+\sum_{k=0}^{a-1}(a-k)\zeta_{n,k}\right]I_{ba}\left(s\left(R_{mn}^{13}/C\right)\right)+\frac{b_{mn}^{13}}{\varepsilon}\sum_{a=0}^{b-1}\zeta_{n,a}I_{ba}\left(s\left(R_{mn}^{13}/C\right)\right)\right] \\ +\displaystyle\sum_{n=1}^{N_w}-sc_{mn}^{23}\sum_{k=0}^{b-1}\upsilon_{n,k}I_{bb}\left(s\left(R_{mn}^{23}/C\right)\right)+\sum_{n=1}^{N_w}-sc_{mn}^{23}\sum_{a=0}^{b-1}\left[\frac{1}{2}\upsilon_{n,a}+\sum_{k=0}^{a-1}\upsilon_{n,k}\right]I_{ba}\left(s\left(R_{mn}^{23}/C\right)\right) \end{array}\right] \tag{B3}$$

REFERENCES

1. Seidel, D. B., D. G. Dudley, and C. M. Butler, "Aperture excitation of a wire in a rectangular cavity," *Interaction Notes*, Note 345, June 1977.

2. Bailin, M. and D. K. Cheng, "Transient electromagnetic fields coupled into a conducting cavity through a slot aperture," *Scientia Sinica (Series A)*, Vol. XXVII, No. 7, 775–784, July 1984.
3. Wen, G., "Time-domain theory of metal cavity resonator," *Progress In Electromagnetics Research*, Vol. 78, 219–253, 2008.
4. Zhang, G.-H., M. Xia, and X.-M. Jiang, "Transient analysis of wire structures using time domain integral equation method with exact matrix elements," *Progress In Electromagnetics Research*, Vol. 92, 281–293, 2009.
5. Zhang, G.-H., M. Xia, and C. H. Chan, "Time domain integral equation approach for analysis of transient responses by metallic-dielectric composite bodies," *Progress In Electromagnetics Research*, Vol. 87, 1–14, 2008.
6. Rao, S. M., *Time Domain Electromagnetics*, Academic Press Series in Engineering, Auburn, 1999.
7. Pisharody, G., R. A. Wildman, and D. S. Weile, "Accurate solution of time domain integral equations using higher order vector bases and bandlimited extrapolation," *IEEE Antennas and Propagation Society International Symposium*, Vol. 3, 555–558, 2003.
8. Weile, D. S., G. Pisharody, N. W. Chen, B. Shanker, and E. Michielssen, "A novel scheme for the solution of the time-domain integral equations of electromagnetics," *IEEE Trans. on Antennas and Propagat.*, Vol. 52, No. 1, 283–295, January 2004.
9. Jung, B. H., T. K. Sarkar, Z. Ji, and Y. S. Chung, "A stable solution of time domain electric field integral equation," IEEE, 2002.
10. Ji, Z., T. K. Sarkar, B. H. Jung, Y. S. Chung, M. S. Palma, and M. Yua, "A stable solution of time domain electric field integral equation for thin-wire antennas using the Laguerre Polynomials," *IEEE Trans. on Antennas and Propagat.*, Vol. 52, No. 10, 2641–2649, October 2004.
11. Jung, B. H., Y.-S. Chung, and T. K. Sarkar, "Time-domain EFIE, MFIE, and CFIE formulations using Laguerre Polynomials as temporal basis functions for the analysis of transient scattering from arbitrary shaped conducting structures," *Progress In Electromagnetics Research*, Vol. 39, 1–45, 2003.
12. Jung, B. H., T. K. Sarkar, Z. Ji, S. Jang, and K. Kim, "Transient electromagnetic scattering from dielectric objects using the electric field integral equation with Laguerre Polynomials as temporal basis functions," *IEEE Trans. on Antennas and Propagat.*, Vol. 52, No. 9, 2329–2340, September 2004.
13. Lacik, J. and Z. Raida, "Modeling microwave structures in time domain using Laguerre Polynomials," *Radioengineering*, Vol. 15, No. 3, September 2006.
14. Mei, Z., Y. Zhang, X. Zhao, B. H. Jung, T. K. Sarker, and M. Salazar-Palma, "Choice of the scaling Factor in a marching-on-in-degree time domain technique based on the associated Laguerre Functions," *IEEE Trans. on Antennas and Propagat.*, Vol. 60, No. 9, 4463–4467, September 2012.
15. Guan, X., S. Wang, Y. Su, and J. Mao, "A method to reduce the oscillations of solution of time domain integral equation using Laguerre Polynomials" *PIERS Online*, Vol. 3, No. 6, 784–789, 2007.
16. Gibson, W. C., *The Method of Moments in Electromagnetics*, 33–62, Chapman & Hall/CRC, US, 2008.
17. Coghetto, M. and C. Offelli, "A procedure for the evaluation of radiated emissions from polygonal wires with the method of moments," *IEEE International Symposium on Electromagnetic Compatibility*, Vol. 1, 334–339, 1999.
18. Chen, K. M., "A mathematical formulation of the equivalence principle," *IEEE Trans. on Microwave Theory and Techniques*, Vol. 37, No. 10, 1576–1581, October 1989.
19. Booysen, A. J., "Aperture theory and the equivalence principle," *IEEE Antennas and Propagation Magazine*, Vol. 45, No. 3, 29–40, June 2003.
20. Booysen, A. J., "Aperture theory and the equivalence theorem," *IEEE Antennas and Propagation Society International Symposium*, Vol. 2, 1258–1261, 1999.